Stem Cell Reports
Article

ISSCR

OPEN ACCESS

Dysregulated ECM remodeling proteins lead to aberrant osteogenesis of Costello syndrome iPSCs

Jong Bin Choi,[1] Joonsun Lee,[1] Minyong Kang,[2] Bumsoo Kim,[1] Younghee Ju,[1] Hyo-Sang Do,[1,3] Han-Wook Yoo,[4] Beom Hee Lee,[4] and Yong-Mahn Han[1,*]

[1]Department of Biological Sciences, KAIST, Daejeon 34141, Republic of Korea
[2]Department of Urology, Samsung Medical Center, Sungkyunkwan University School of Medicine, Seoul 06351, Republic of Korea
[3]Asan Institute for Life Sciences, Asan Medical Center, University of Ulsan College of Medicine, Seoul 05505, Republic of Korea
[4]Department of Pediatrics, Asan Medical Center Children's Hospital, University of Ulsan College of Medicine, Seoul 05505, Republic of Korea
*Correspondence: ymhan@kaist.ac.kr
https://doi.org/10.1016/j.stemcr.2021.06.007

SUMMARY

Costello syndrome (CS) is an autosomal dominant disorder caused by mutations in HRAS. Although CS patients have skeletal abnormalities, the role of mutated HRAS in bone development remains unclear. Here, we use CS induced pluripotent stem cells (iPSCs) undergoing osteogenic differentiation to investigate how dysregulation of extracellular matrix (ECM) remodeling proteins contributes to impaired osteogenesis. Although CS patient-derived iPSCs develop normally to produce mesenchymal stem cells (MSCs), the resulting CS MSCs show defective osteogenesis with reduced alkaline phosphatase activity and lower levels of bone mineralization. We found that hyperactivation of SMAD3 signaling during the osteogenic differentiation of CS MSCs leads to aberrant expression of ECM remodeling proteins such as MMP13, TIMP1, and TIMP2. CS MSCs undergoing osteogenic differentiation also show reduced β-catenin signaling. Knockdown of TIMPs permits normal differentiation of CS MSCs into osteoblasts and enhances β-catenin signaling in a RUNX2-independent manner. Thus, this study demonstrates that enhanced TIMP expression induced by hyperactivated SMAD3 signaling impairs the osteogenic development of CS MSCs via an inactivation of β-catenin signaling.

INTRODUCTION

Costello syndrome (CS) is an example of a RASopathy, a family of genetic disorders caused by RAS/MAPK signaling defects (Tidyman and Rauen, 2009). CS is caused mainly by constitutive activation of RAS signaling resulting from mutations in the Harvey rat sarcoma viral oncogene homolog (HRAS) (Aoki et al., 2005). CS patients frequently have germline heterozygous glycine-to-serine missense mutations at amino acid 12 ($HRAS^{G12S}$). These patients show various clinical phenotypes, including intellectual disability, hypertrophic cardiomyopathy, postnatal growth retardation, short stature, and craniofacial malformations (Costello, 1977; Hennekam, 2003). Although skeletal defects are a common feature in a majority of CS patients (Leoni et al., 2014), the mechanism by which $HRAS^{G12S}$ induces abnormal bone development remains unclear.

Mesenchymal stem cells (MSCs) develop into embryonic bone and are needed to maintain a continuous supply of osteogenic cells for bone remodeling (Bruder et al., 1994). Runt-related transcription factor 2 (RUNX2) plays an important role in the expression of most genes associated with osteogenic differentiation (Ducy et al., 1997). On the other hand, the transcription factor osterix (OSX) modulates the expression of factors downstream of RUNX2, factors like collagen type I, osteocalcin (OCN), and bone sialoprotein (Nakashima et al., 2002). The expression and transcriptional activity of RUNX2 is directly modulated by transforming growth factor β (TGF-β) signaling (Alliston et al., 2001). TGF-β signaling also regulates the expression of extracellular matrix (ECM) remodeling factors important for the osteogenic and chondrogenic differentiation of MSCs (Chen et al., 2012; Rydziel et al., 1997).

ECM remodeling affects developmental processes such as cell differentiation fate, stemness, morphogenesis, cell migration, and apoptosis. It also interacts with growth factors and cytokines (Vu and Werb, 2000). Matrix metalloproteinases (MMPs) and their modulators, the tissue inhibitors of MMPs (TIMPs), are associated with the synthesis and release of the growth factor binding proteins that underlie latent growth factor functions (Kasper et al., 2007; Mott and Werb, 2004). MMPs and TIMPs play important roles in determining the cell fate of MSCs as they differentiate into adipocytes, osteocytes, and chondrocytes (Kasper et al., 2007). Expression of MMP2, MMP13, MMP14, and members of the TIMP family (i.e., TIMP1 and TIMP2) is required for ECM remodeling in the differentiation of MSCs into osteoblasts (Almalki and Agrawal, 2016). MMP2 knockout (KO) mice display craniofacial abnormalities and gradual reduction of bone mineral density with aging (Mosig et al., 2007). Knockdown (KD) of MMP13 in human adipose tissue-derived MSCs suppresses alkaline phosphatase (ALP) activity and mineralization during osteogenic differentiation (Ozeki et al., 2016). MMP14 deficiency leads to a deregulation of collagen turnover, thereby leading to dwarfism and impairment of bone development in mice (Holmbeck et al., 1999). TIMP KO mice show abnormalities in bone growth, such as long bone growth

plate closure defects, limb shortening, epiphyseal distortion, and widespread chondrodysplasia (Saw et al., 2019). Nevertheless, the roles that ECM remodeling factors like the TIMPs and MMPs play in human osteogenesis remain poorly understood. In this study, we have examined the relationship between the osteogenic activity of CS MSCs and ECM remodeling. In addition, TIMP1 and TIMP2 can function as ligands that regulate Wnt/β-catenin signaling (Egea et al., 2012; Xia and Wu, 2015). Wnt/β-catenin signaling plays an important role in bone development via two mechanisms: it promotes osteogenesis and suppresses chondrogenesis (Day et al., 2005; Krishnan et al., 2006).

Here, we used CS induced pluripotent stem cells (iPSCs) to investigate the effect of the $HRAS^{G12S}$ mutation on bone development. During osteogenic differentiation, CS MSCs show enhanced SMAD3 signaling activity and altered expression of ECM remodeling proteins such as TIMP1, TIMP2, and MMP13. Intriguingly, we found that elevated p-SMAD3 levels do not affect RUNX2 expression during osteogenic development. Transfection of TIMP-specific small interfering RNAs (siRNAs) rescues the osteogenic activity of CS MSCs and enhances their expression of OSX. Furthermore, KD of TIMP1 rescues β-catenin signaling in CS MSCs during osteogenic development *in vitro*. Our results suggest TIMP overexpression underlies the abnormal skeletal abnormalities of CS patients during early development in a RUNX2-independent manner.

RESULTS

CS-iPSC-derived MSCs show poor osteoblast differentiation potency *in vitro*

As with wild-type (WT) iPSCs, we found that CS iPSCs generated from three different CS patients express normal levels of pluripotency-associated markers (Figure S1B) and can form three germ layers (Figure S1C). These CS iPSCs can differentiate into MSCs prior to osteogenic differentiation just like WT iPSCs. Both WT MSCs and CS MSCs exhibit high expression of MSC-positive markers (i.e., CD73, CD90, and CD105) and low expression of MSC-negative markers (i.e., CD34, CD45, and HLA-DR) (Figure 1A) while maintaining normal morphology (Figure S1D). As expected, we found that CS MSCs show significantly more HRAS activity than WT MSCs, which also results in elevated phosphorylated extracellular-signal-regulated kinase (p-ERK) levels (Figure 1B). During osteogenic differentiation, CS MSCs show reduced ALP activity and weak alizarin red S (AR-S) and von Kossa (VK) staining, implying reduced mineralization (Figure 1C). Like WT MSCs, in contrast, CS MSCs differentiate normally into chondrocytes and adipocytes (Figures S1E and S1F). In addition, WT MSCs and CS MSCs subjected to 5-ethynyl-2′-deoxyuridine (EdU) assays show no difference in proliferation rate during osteogenesis (Figure S1G). These results demonstrate that CS MSCs show impaired competence to differentiate into osteoblasts despite being normal in appearance and showing normal expression of MSC surface markers.

Enhanced SMAD3 signaling impairs osteogenesis in CS MSCs

The regulation of bone homeostasis and embryonic skeletal development requires TGF-β signaling (Wu et al., 2016). We previously reported that a BRAF mutation causing the RASopathy known as cardiac-facial-cutaneous (CFC) syndrome leads to defective osteogenesis in CFC MSCs due to the hyperactivation of ERK and TGF-β signaling (Choi et al., 2017b). Thus, we asked whether the same signaling pathways may also be dysregulated in CS MSCs during osteogenesis *in vitro*. As expected, we observed enhanced p-ERK in CS MSCs at day 7 of osteogenic induction. Although CS osteoblasts show similar levels of p-SMAD2, they show increased p-SMAD3 levels compared with WT osteoblasts (Figure 2A). In addition, CS osteoblasts show significantly reduced expression (transcriptional and translational) of the osteogenic markers OSX, *OCN*, and collagen type I, but not *RUNX2* (Figures S2A and S2B). To correlate ERK signaling with SMAD signaling, we incubated CS MSCs with a p-ERK inhibitor (U0126) during osteogenic differentiation. This inhibition of ERK signaling in CS MSCs during osteogenic differentiation reduces both their p-ERK and their p-SMAD3 levels, but not their p-SMAD2 levels (Figure 2B). This result implies that ERK activity influences SMAD3 but not SMAD2 signaling in CS MSCs during osteogenesis. Interestingly, we found that inhibition of TGF-β signaling does not influence p-ERK activity during osteogenesis by CS MSCs (Figure 2C). We also found that inhibition of ERK signaling increases ALP activity but does not rescue the mineralization defect of CS osteoblasts (Figure S2D). Inhibition of TGF-β signaling, however, enhances both ALP activity and mineralization in CS osteoblasts compared with nontreated controls (Figure S2E). When we transfected a constitutively active form of SMAD3 (SMAD3CA) into WT MSCs during osteogenic differentiation, the transfected cells showed low ALP activity and weak AR-S staining, indicating insufficient osteogenesis (Figure 2D). In addition, the expression of PAI-1—a known SMAD3 target gene (Hua et al., 1999)—was significantly higher in SMAD3CA-transfected osteoblasts compared with WT osteoblasts (Figure S2F). As we observed with CS osteoblasts, these transfected cells showed lower expression of all the osteogenic markers we tested except RUNX2 (Figure S2F). Moreover, constitutive activation of

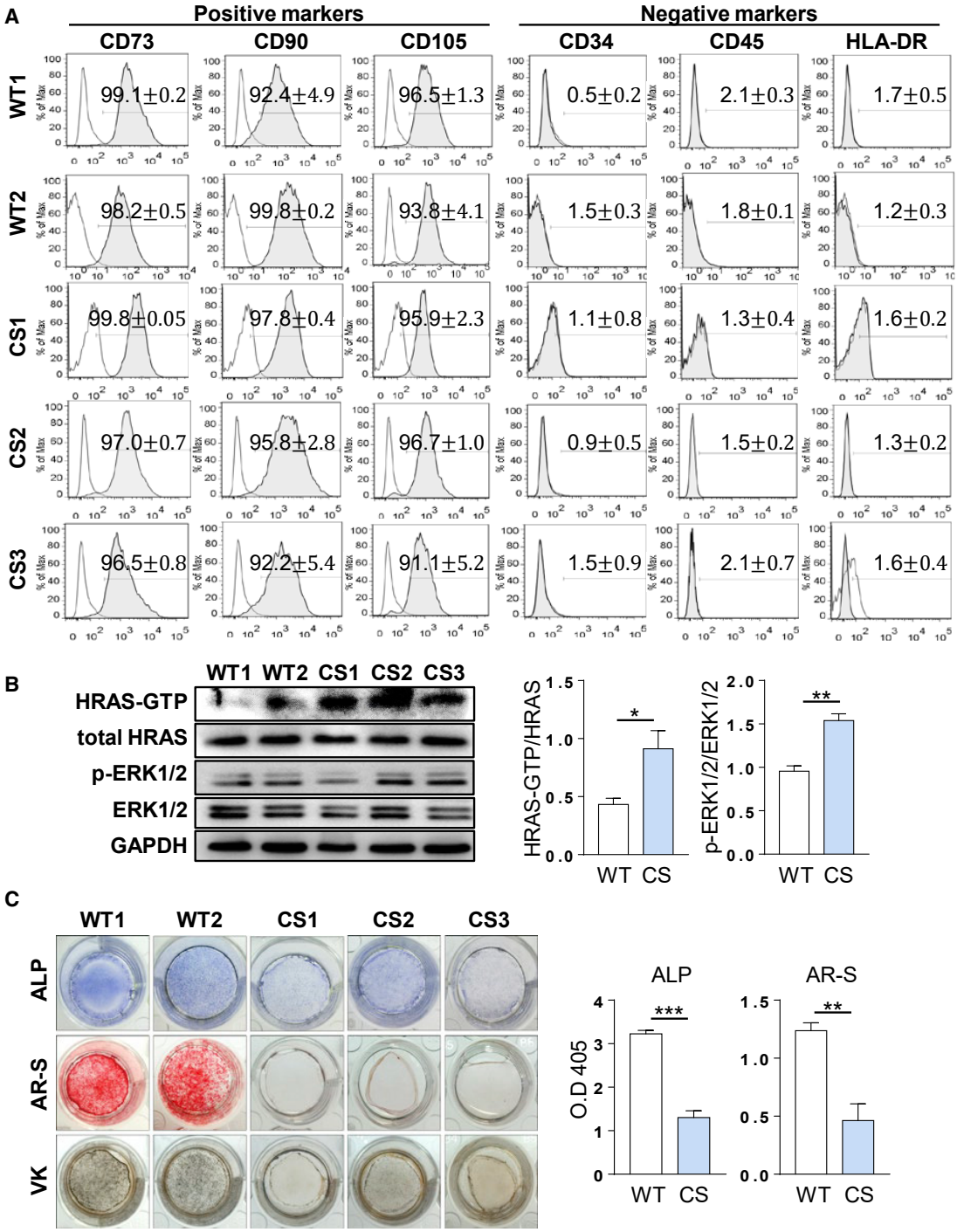

Figure 1. Defective osteogenic differentiation of CS MSCs

(A) Normal expression of MSC surface markers in CS MSCs. WT, wild type; CS, Costello syndrome.

(B) Enhanced activities of HRAS-GTP and ERK in CS MSCs. Data are presented as means ± SEM (n = 3). *p < 0.05; **p < 0.01.

(C) Reduced ALP activity and calcium deposition in CS MSCs during osteogenic differentiation. Data are presented as means ± SEM (n = 3). **p < 0.01; ***p < 0.001 (Student's t test). ALP, alkaline phosphatase; AR-S, alizarin red staining; VK, von Kossa staining.

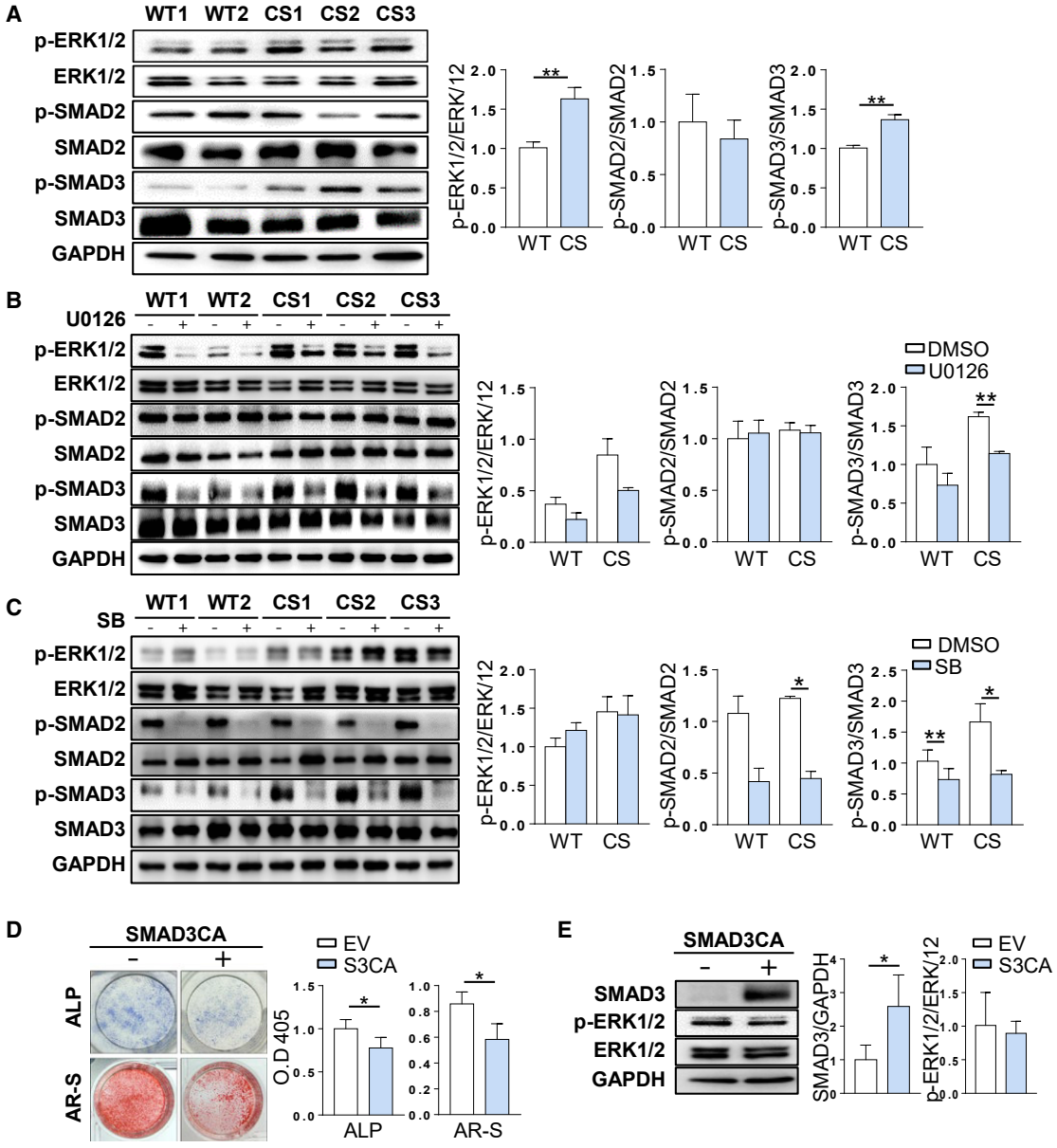

Figure 2. Enhanced SMAD3 signaling impairs osteogenic differentiation of CS MSCs

(A) Elevated levels of p-ERK and p-SMAD3 in CS osteoblasts (n = 4).

(B) Suppression of SMAD3 signaling in CS MSCs during osteogenesis by treatment with an ERK inhibitor (U0126, 10 μM) (n = 3).

(C) Inhibition of TGF-β signaling in the osteogenic development of CS MSCs does not affect ERK signaling activity (n = 4). SB, SB431542.

(D) Recapitulation of osteogenic defects in WT MSCs by SMAD3CA overexpression. SMAD3CA, constitutively active form of SMAD3 (n = 3). ALP, alkaline phosphatase; AR-S, alizarin red staining; EV, empty vector; S3CA, SMAD3CA.

(E) SMAD3CA overexpression does not affect ERK activity in WT MSCs (n = 4). EV, empty vector; S3CA, SMAD3CA.

Data information: in (A–C), data are presented as means ± SEM. *p < 0.05; **p < 0.01 (Student's t test). In (D and E), data are presented as means ± SD. *p < 0.05 (Student's t test).

SMAD3 signaling does not seem to affect p-ERK signaling during osteogenic development *in vitro* (Figure 2E). Thus, hyperactivated ERK signaling seems to irreversibly increase SMAD3 signaling activity in CS MSCs during osteogenesis. Together, our results suggest that hyperactivated SMAD3 signaling caused by increased ERK signaling is the main contributor to the defective osteogenesis of CS MSCs.

Enhanced SMAD3 signaling in CS MSCs alters the expression of ECM remodeling proteins and disrupts osteogenesis in a RUNX2-independent manner

Hyperactivated SMAD3 signaling reportedly represses RUNX2 expression and transcriptional activity in mouse primary osteoblasts and osteosarcoma cells (Alliston et al., 2001). Despite the enhanced SMAD3 signaling we observed in this study, we did not observe reduced expression of RUNX2 in CS MSCs during osteogenesis (Figures S2A and S2B). In addition, we found similar RUNX2 transcriptional activity during osteogenic development between CS and WT MSCs (Figure S2C). Thus, we hypothesized that SMAD3 signaling may contribute to the defective osteogenesis of CS MSCs via a RUNX2-independent mechanism. SMAD3 signaling is known to modulate the expression of ECM remodeling proteins in mesenchymal cells (Chen et al., 2012; Verrecchia and Mauviel, 2002; Yao et al., 2017), and ECM remodeling is required for bone maturation during skeletal development (Lu et al., 2011). Thus, we decided to examine the expression of key osteogenesis-related ECM remodeling proteins in CS osteoblasts. We found reduced expression of MMP13 and elevated expression of the MMP modulators (TIMP1 and TIMP2) in CS osteoblasts compared with WT osteoblasts (Figure 3A). In addition, CS osteoblasts secrete significantly more TIMP1 and TIMP2 in serum-free medium than WT osteoblasts (Figure S3A). We next asked whether aberrant expression of ECM proteins is associated with the impaired osteogenesis of CS MSCs. We found that treatment of CS osteoblasts with recombinant human MMP13 (rhMMP13; 5 μM) does not effectively rescue their ALP activity (Figures S3B and S3C) or mineralization defects (Figures 3B and S3D). In contrast, transfection of CS osteoblasts with TIMP1- and TIMP2-specific siRNAs does effectively rescue their ALP activity (Figures S3B and S3C) and mineralization (Figures 3B and S3D) defects. We also found that the combination of rhMMP13 treatment with TIMP-specific siRNA transfection induces a synergistic increase in CS-osteoblast mineralization, but not ALP activity (Figures 3B and S3D). These results demonstrate that upregulation of TIMP1 and/or TIMP2 leads to defective osteogenesis in CS MSCs. Intriguingly, inhibition of TGF-β signaling enhances the expression of MMP13 and reduces the expression of TIMP1 and TIMP2 as CS MSCs undergo osteogenesis (Figure 3C). However, while inhibition of TGF-β signaling upregulates OSX expression in CS osteoblasts, it does not affect RUNX2 expression (Figure 3C). WT MSCs transfected with SMAD3CA show reduced expression of MMP13 and OSX but enhanced expression of TIMP1 and TIMP2 (Figure 3D). Thus, TGF-β signaling is likely involved in the expression of TIMP1, TIMP2, and MMP13 in CS MSCs during osteogenic differentiation. In addition, the transfection of TIMP1- or TIMP2-specific siRNAs increases OSX expression during the osteogenic differentiation of CS MSCs, but treatment with rhMMP13 does not (Figures 3E and S3E). In addition, we did not observe any changes in RUNX2 expression regardless of the experimental conditions. Our findings suggest that aberrant ECM remodeling protein expression contributes to the defective osteogenic differentiation of CS MSCs independent of RUNX2.

Overexpression of TIMP1 in CS MSCs inhibits osteogenesis by reducing β-catenin signaling

TIMP1 binding to CD63 on the surface of human MSCs is known to enhance AXIN2 activity, thereby suppressing β-catenin signaling (Egea et al., 2012). Active β-catenin acts as a key regulator in the expression of OSX during osteogenesis (Choi et al., 2017a; Felber et al., 2015; Liu et al., 2015). Thus, we examined the activity of β-catenin signaling in CS MSCs during osteogenic development. We found enhanced AXIN2 expression and reduced active β-catenin in CS osteoblasts compared with WT osteoblasts (Figure 4A), while the levels of other complex proteins (APC and GSK3β) remained similar. In an immunofluorescence analysis, we also found reduced active β-catenin in CS osteoblasts compared with WT (Figure S4A). CS osteoblasts also show reduced levels of the β-catenin target gene cyclin D1, but WT levels of CD63 expression (Figure 4A). Upon treatment with the AXIN2 inhibitor SKL2001, we observed a significant increase in active β-catenin and OSX in CS MSCs during osteogenic differentiation, but this did not affect RUNX2 expression (Figure 4B). Furthermore, we found that AXIN2 inhibition restores ALP activity and mineralization in CS MSCs during osteogenesis (Figure S4B). Thus, inactivation of β-catenin signaling via a hyperactivation of AXIN2 seems to cause aberrant osteogenic differentiation of CS MSCs. Next, to determine whether TIMP1 modulates β-catenin signaling, we transfected MSCs with TIMP1-specific siRNAs and/or SMAD3CA expression vectors during *in vitro* osteogenic differentiation. We found that TIMP1 KD in CS MSCs elevates the activity of β-catenin during osteogenic development (Figure S4C). Furthermore, TIMP1 KD in WT MSCs during osteogenic differentiation reduces AXIN2 expression, but enhances β-catenin activity (active β-catenin and cyclin D1), regardless of SMAD3CA expression (Figure 4C). TIMP1 KD also increases the expression of OSX and MMP13 in the transfected cells without affecting RUNX2 expression. Thus, it is obvious that TIMP1 is involved in osteogenesis, regulating β-catenin signaling independent of RUNX2. TIMP1 KD in WT MSCs during osteogenesis restores the ALP activity and mineralization defects caused by SMAD3CA transfection (Figure 4D). Together, our findings demonstrate that TIMP1 overexpression causes aberrant osteogenesis in CS MSCs via a downregulation of β-catenin signaling.

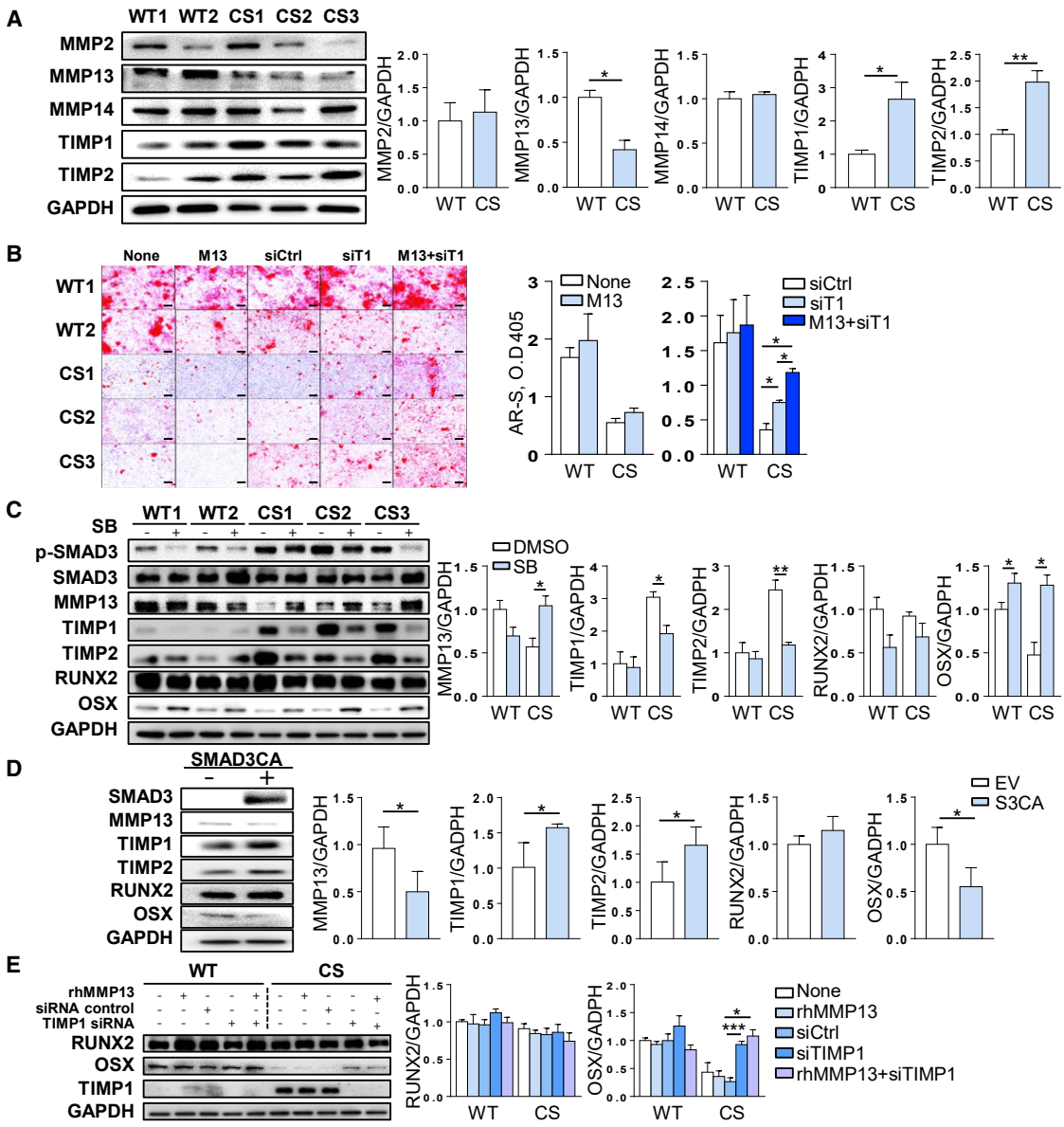

Figure 3. Aberrant expression of ECM remodeling proteins in CS osteoblasts

(A) Dysregulation of ECM remodeling protein expression in CS osteoblasts. CS osteoblasts show reduced expression of MMP13 and increased expression of TIMP1 and TIMP2 (n = 3).

(B) Rescue of mineralization in CS MSCs upon transfection with TIMP1-specific siRNAs (n = 3). AR-S, alizarin red staining; M13, recombinant human MMP13; siCtrl, siRNA control; siT1, TIMP1 siRNA; O.D, optical density. Scale bars: 200 μm.

(C) Inhibition of SMAD3 signaling alters the expression of ECM remodeling proteins in CS MSCs. SMAD3 inhibition increases MMP13 expression and reduces TIMP1 and TIMP2 expression in CS osteoblasts (n = 4).

(D) Transfection of WT MSCs with SMAD3CA vectors affects the expression of ECM remodeling proteins. SMAD3CA overexpression in WT MSCs during osteogenic differentiation reduces MMP13 expression and enhances TIMP1 and TIMP2 expression (n = 4). EV, empty vector; S3CA, SMAD3CA.

(E) TIMP1 KD in CS MSCs during osteogenic development affects their expression of OSX. TIMP1-specific siRNAs enhance OSX expression independent of RUNX2 (n = 3). rhMMP13, recombinant human MMP13; siCtrl, siRNA control; siTIMP1, TIMP1 siRNA.

Data information: band intensities for the indicated proteins were measured using ImageJ and then normalized to GAPDH controls. In (A–C and E), data are presented as means ± SEM. *p < 0.05; **p < 0.01; ***p < 0.001 (Student's t test). In (D), data are presented as means ± SD. *p < 0.05 (Student's t test).

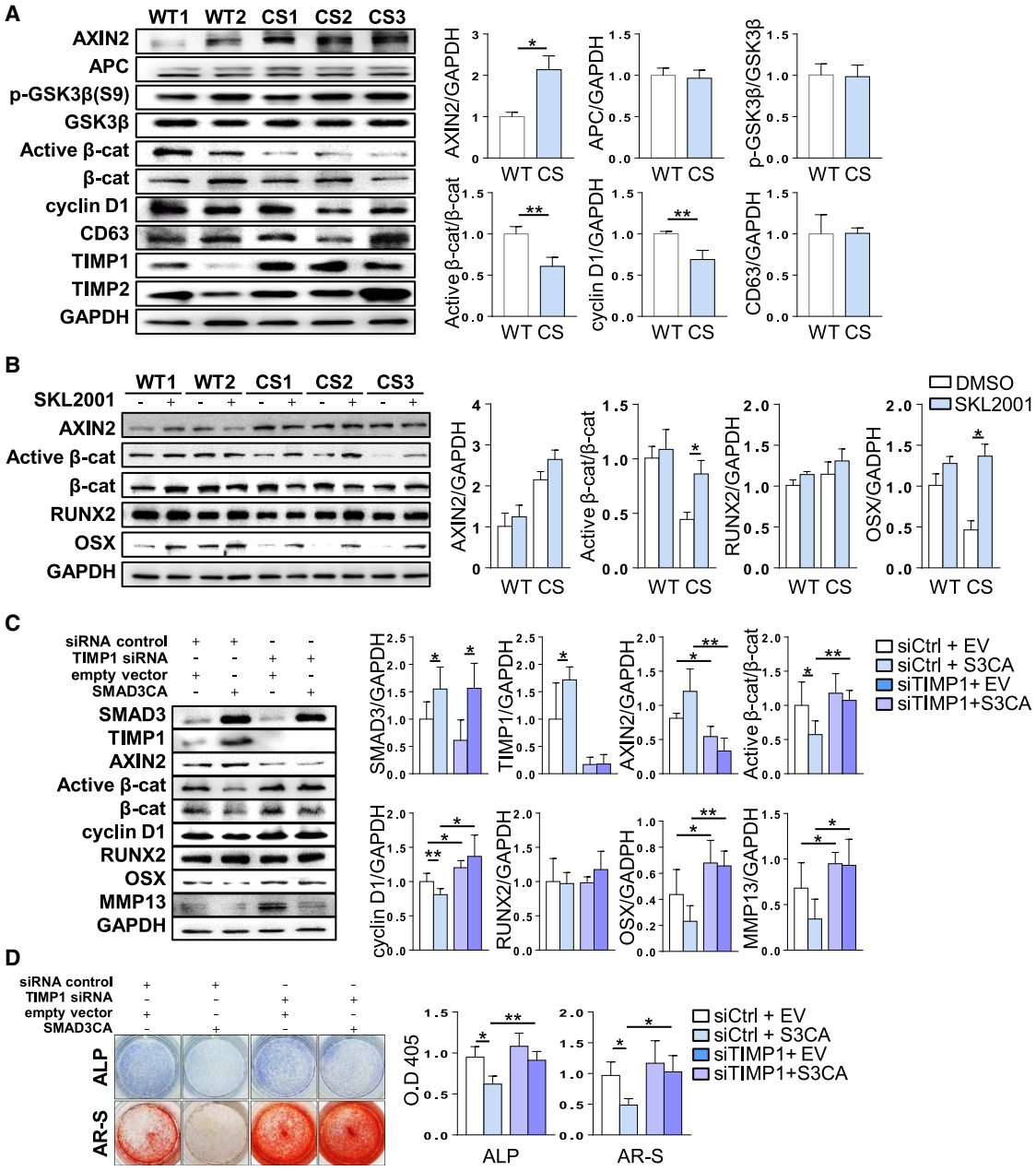

Figure 4. Reduced β-catenin signaling in CS osteoblasts

(A) Increased AXIN2 expression and decreased β-catenin signaling in CS osteoblasts. β-cat, β-catenin (n = 4).

(B) Treatment with the AXIN2 inhibitor SKL2001 (40 μM) increases active β-catenin and OSX expression in CS MSCs during osteogenic differentiation (n = 3).

(C) Relationship of TIMP1 and β-catenin signaling in osteogenic development. TIMP1 KD reduces AXIN2 expression, enhances β-catenin activity (active β-catenin and cyclin D1), and increases OSX expression in WT MSCs during osteogenic differentiation (n = 5). siCtrl, siRNA control; siTIMP1, TIMP1 siRNA; EV, empty vector; S3CA, SMAD3CA.

(D) Relationship of TIMP1 and SMAD3 signaling in osteogenic development. TIMP1 KD rescues ALP activity and AR-S staining in WT MSCs transfected with SMAD3CA vectors (n = 4). ALP, alkaline phosphatase; AR-S, alizarin red staining; siCtrl, siRNA control; siTIMP1, TIMP1 siRNA; EV, empty vector; S3CA, SMAD3CA.

Data information: in (A and B), data are presented as means ± SEM. *p < 0.05; **p < 0.01 (Student's t test). In (C and D), data are presented as means ± SD. *p < 0.05; **p < 0.01 (Student's t test).

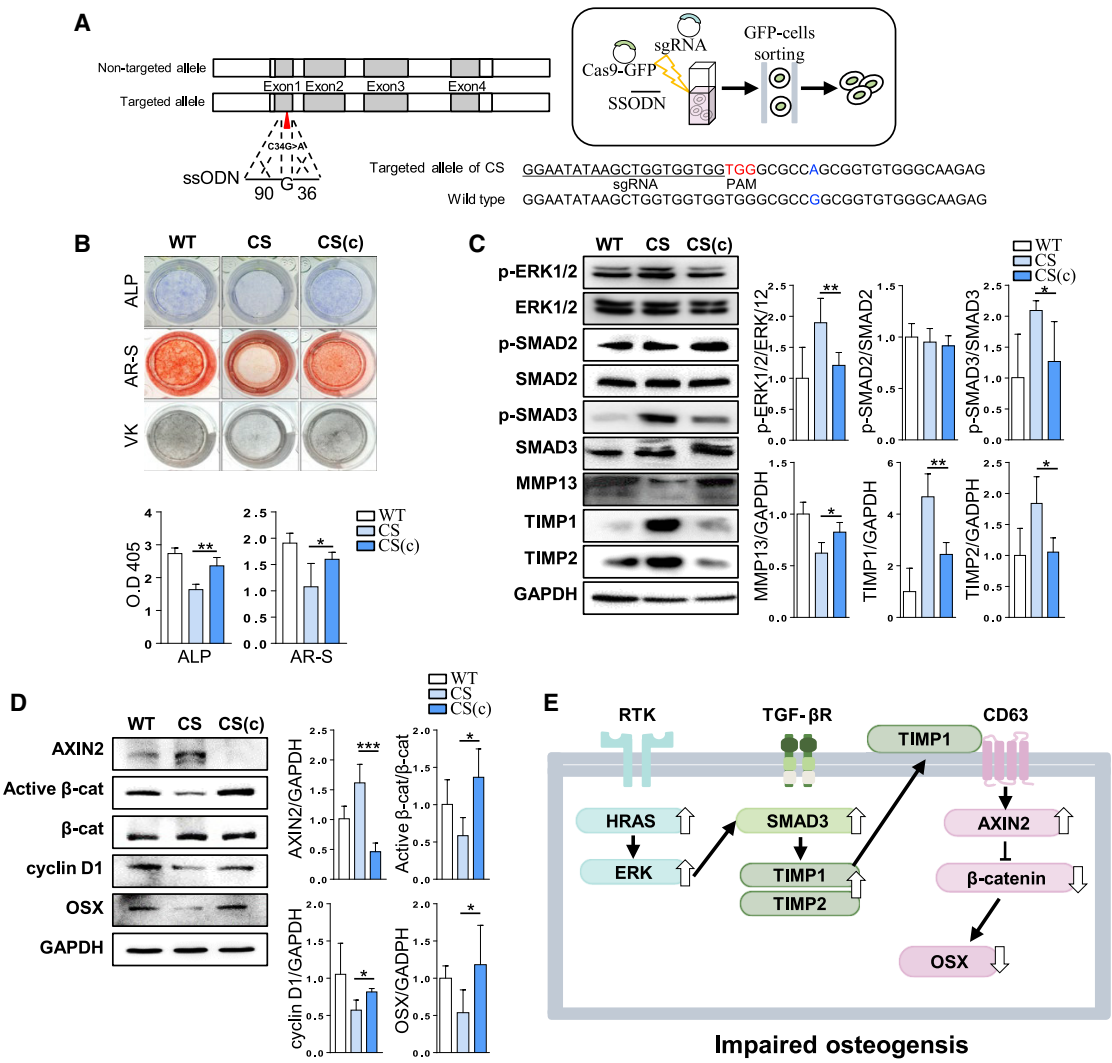

Figure 5. Correction of HRAS^{G12S} in CS iPSCs using the CRISPR-Cas9 system

(A) Correction of an HRAS mutation in CS iPSCs using the CRISPR-Cas9 system.

(B) Increased ALP activity and AR-S staining in CS(c) osteoblasts (n = 4). ALP, alkaline phosphatase; AR-S, alizarin red staining.

(C) Reduced p-ERK and p-SMAD3 with normal expression of ECM remodeling proteins (MMP13, TIMP1, and TIMP2) in CS(c) osteoblasts (n = 4).

(D) Reduced expression of AXIN2 and enhanced β-catenin activity (active β-catenin and cyclin D1) in CS(c) osteoblasts (n = 4).

(E) Modeling the impaired osteogenesis of CS MSCs. RTK, receptor tyrosine kinase; TGF-βR, TGF-β receptor.

Data information: in (B–D), data are presented as means ± SD. *p < 0.05; **p < 0.01; ***p < 0.001 (Student's t test). CS(c), corrected CS iPSCs.

Correction of HRAS^{G12S} using CRISPR-Cas9 validates a model for the impaired osteogenesis of CS MSCs

To confirm whether the active HRAS^{G12S} mutation really causes aberrant osteogenesis, the HRAS mutation of CS iPSCs was corrected using the CRISPR-Cas9 system. CS iPSCs with c.34G > A mutation were electroporated with single guide RNA (sgRNA) plasmids, CRISPR-Cas9-GFP plasmids, and single-stranded oligodeoxynucleotides (ssODNs). Transformed cells (GFP-positive cells) were selected by fluorescence-activated cell-sorting (FACS) isolation and cultured until colony formation (Figure 5A). Of the 50 CS iPSC colonies we tested, we found one corrected clone that expressed normal levels of the pluripotency-associated markers (Figure S5A) and had a normal karyotype (Figure S5B). The clone showed no evidence of mutation in the top four potential off-target sites (Figure S5C).

MSCs derived from these corrected CS iPSCs (CS(cor) MSCs) showed normal expression of MSC positive and negative markers (Figure S5D), in addition to reduced HRAS activity and p-ERK levels (Figure S5E). These CS(cor) MSCs were capable of differentiating into normal osteoblasts with higher levels of ALP activity and mineralization than their parent CS MSCs (Figure 5B). As expected, $HRAS^{G12S}$ correction rescues the hyperactivated p-SMAD3 signaling and the dysregulation of ECM remodeling protein expression in CS osteoblasts (Figure 5C). We found that $HRAS^{G12S}$ correction also rescues β-catenin signaling and OSX expression (Figure 5D). Our results indicate that $HRAS^{G12S}$ impairs osteogenesis by affecting SMAD3/β-catenin signaling, thereby dysregulating ECM remodeling protein expression.

DISCUSSION

Here we suggest a cellular model underlying the impaired bone development of CS patients. We demonstrate for the first time that dysregulation of ECM remodeling is associated with defective osteogenesis using CS iPSCs. During the osteogenic differentiation of CS MSCs, mutated HRAS hyperactivates both ERK signaling and SMAD3 signaling. This enhanced SMAD3 activity leads to overexpression of TIMP1 and TIMP2. KD of TIMP1 or TIMP2 rescues the defective ALP activity and mineralization capacity of CS MSCs during osteogenic differentiation *in vitro*.

We previously reported that enhanced SMAD2 signaling contributes to the impaired osteogenic differentiation of CFC MSCs (Choi et al., 2017b). Here, we observed hyperactivation of SMAD3 signaling in CS MSCs during osteogenic development (Figure 2A). Thus, TGF-β signaling differentially contributes to the osteogenic development of CS and CFC MSCs. SMAD2 and SMAD3 reportedly also show differential sensitivity to TGF-β signaling in the early lineage specifications of mouse embryonic development. In teratomas, overexpression of SMAD2 downregulates neural gene expression and upregulates mesodermal gene expression, while overexpression of SMAD3 upregulates neural gene expression and downregulates mesodermal gene expression (Liu et al., 2016). Collectively, our results suggest that CS and CFC patients may have minor differences in bone development, despite both conditions being members of the same RASopathy family of disorders.

SMAD3 activity represses osteogenic development by reducing the expression of RUNX2 and OCN in mouse primary osteoblasts (Alliston et al., 2001). In this study, however, both CS MSCs and WT MSCs overexpressing the SMAD3CA show steady expression of RUNX2 throughout osteogenic differentiation (Figures 3C and 3D). Thus, RUNX2 expression seems to be independent of SMAD3 activity in CS MSCs. In addition, WT and CS osteoblasts do not show a significant difference in the expression of *TGF-β* or *Activin A* (Figure S2G). This means the activation of TGF-β signaling we observed in CS osteoblasts arises from enhanced p-ERK, rather than increased levels of ligand. In addition, we found via western blot that CS MSCs undergoing osteogenesis show inhibition of ERK signaling and slightly increased expression of RUNX2 (Figure S2H). It is therefore conceivable that the enhanced ERK activity of CS MSCs undergoing osteogenesis does not affect RUNX2 expression.

Treatment with the ERK inhibitor PD0325901 reportedly rescues the low density of mineralized enamel secreted by ameloblasts in CS ($HRAS^{G12V}$) mice (Goodwin et al., 2014). In this study, we found that treatment with the ERK inhibitor U0126 rescued the ALP activity of CS MSCs undergoing osteogenic differentiation but failed to restore their decreased mineralization (Figure S2D). This difference suggests that ERK signaling regulates mineralization during bone development in a cell-type-specific manner. Moreover, the effects of RAS-ERK on osteogenesis remain controversial because of variations in experimental methodology and the use of diverse cell lines and primary cells at various stages of osteogenic development (Schindeler and Little, 2006). Our results indicate that ERK signaling is not a crucial effector of mineralization in CS MSCs undergoing osteogenic development.

Next, we found aberrant expression of ECM remodeling proteins in CS osteoblasts. Similar dysregulation of ECM signaling has also been reported in CS astrocytes derived from CS iPSCs (Krencik et al., 2015). CS osteoblasts express higher levels of TIMP1 and TIMP2 but lower levels of MMP13 than WT osteoblasts (Figure 3A). Moreover, we found that KD of TIMP1 or TIMP2 led to increased ALP activity and mineralization in CS MSCs during osteogenic differentiation (Figures 3B and S3B–S3D). TIMP3 is reportedly modulated by both the ERK1/2 and the SMAD3 signaling pathways (Leivonen et al., 2013). We found an enrichment of TIMP3 transcripts in CS osteoblasts compared with WT osteoblasts (Figure S3G). Nevertheless, we decided to investigate the roles of TIMP1 and TIMP2 in this study because they are key regulators of ECM remodeling in MSCs during osteogenic development (Almalki and Agrawal, 2016). These results indicate that aberrant expression of ECM remodeling proteins is responsible for the defective osteogenic development of CS MSCs. In addition, we found that osteogenic differentiation of CS MSCs is unaffected by rhMMP13 treatment (Figures S3B and S3C). Unlike what we observed with mineralization, we found that combined treatment with TIMP1- or TIMP2-specific siRNAs and rhMMP13 did not produce a synergistic effect on ALP activity (Figures 3B and S3D). This difference seems to be due to the temporal role of MMP13 in bone development. MMP13 reportedly restructures the collagen matrix for mineralization in long bone

development (Page-McCaw et al., 2007). OSX KO mouse osteoblasts reportedly show a specific downregulation of MMP13 (Zhang et al., 2012). Because OSX is also reduced in CS osteoblasts (Figures S2A and S2B), we suspected that the reduction of MMP13 is secondary to the reduced levels of OSX in CS osteoblasts. When we knocked down TIMP1 in WT MSCs, we observed an increase in the expression of MMP13 and OSX (Figure 4C). During osteogenesis, OSX activates the expression of collagen type I, the most abundant ECM molecule in the bone matrix (Boskey, 2013; Nakashima et al., 2002). In this study, we found that the reduced expression of OSX in CS osteoblasts compared with WT osteoblasts leads to lower expression of pro-collagen type I (Figures S2A and S2B). Regardless, CS and WT osteoblasts show similar levels of fibrillar collagen type I deposition (Figure S3F). This homeostatic deposition of fibrillar collagen type I seems to be responsible for the TIMP overexpression-induced reduction of MMP13 in CS osteoblasts. MMPs, which are inhibited by TIMPs, liberate active TGF-β from large latent complex binding to several ECM proteins, such as fibrillin-1, fibronectin, and vitronectin (Wipff and Hinz, 2008). Although latent TGF-β/BMPs are highly activated in Fbn1-null mouse osteoblasts (Nistala et al., 2010), we found enhanced TGF-β and reduced BMP1/5/9 in CS MSCs during osteogenesis (Figures 2A and S4E). Because the transcription levels of TGF-β ligands in CS osteoblasts are similar to those of WT osteoblasts (Figure S2G), it is likely that TGF-β activity is independent of the ligand expression. Collectively, it is obvious that TIMP overexpression is a crucial factor leading to the defective osteogenesis of CS MSCs.

TIMP1 acts as a ligand to inhibit β-catenin signaling independent of MMP activity. TIMP1 KD in WT MSCs reportedly reduces their expression of AXIN2 and activates β-catenin signaling, increasing osteogenesis (Egea et al., 2012). In contrast, TIMP1 overexpression increases AXIN2 expression and inactivates β-catenin signaling in CS MSCs during osteogenic differentiation (Figure 4A). As shown in Figure S4D, rhTIMP1 transduction increased AXIN2, decreased β-catenin activity, and decreased MMP13/OSX expression in WT MSCs during osteogenic differentiation, all leading to reduced ALP activity and mineralization. Combined treatment with rhTIMP1 and an AXIN2 inhibitor, however, did not affect MMP13 expression. Thus, TIMP1 alone does not contribute to reducing MMP13. In addition, we observed a significant reduction in p-SMAD1/5/9 in CS osteoblasts (Figure S4E) that probably results from an increase in AXIN2. This is because AXIN2 inhibits the BMP pathway by reducing β-catenin activity (Yan et al., 2009). Interestingly, CS MSCs also show increased osteogenic activity upon inhibition of AXIN2 (Figure S4B). Furthermore, KD of TIMP1 in WT MSCs transfected with SMAD3CA vectors reduces their expression of AXIN2 and activates β-catenin signaling (Figure 4C). Thus, the overexpression of TIMPs is clearly responsible for reduced β-catenin signaling in CS osteoblasts.

In conclusion, we suggest a model for the defective osteogenesis of CS MSCs that implicates ECM-associated molecules and their associated signaling pathways (Figure 5E). Briefly, we found that mutated $HRAS^{G12S}$ enhances both ERK and SMAD3 signaling in CS MSCs during osteogenic differentiation. Elevated p-SMAD3 leads to aberrant expression of ECM remodeling proteins in CS osteoblasts. In particular, TIMP overexpression reduces β-catenin activity, which disrupts the osteogenic development of CS MSCs. This model provides new insights into the mechanisms by which mutated $HRAS^{G12S}$ induces the bone abnormalities observed in CS patients.

EXPERIMENTAL PROCEDURES

Generation and maintenance of CS iPSCs

CS fibroblasts were biopsied from three patients via a protocol approved by the Asan Medical Center institutional review board (2011-0451). The institutional review board of KAIST (KH2016-52) approved the culture and generation of human iPSCs. Human iPSCs were generated from fibroblasts of each CS patient (CS iPSCs) using Yamanaka's factors (Takahashi et al., 2007). CS patient fibroblasts were a gift from the Asan Medical Center (Table S1). Each of the three patients had a point mutation (c.34G > A) in the *HRAS* gene located at chromosome 11p15 that resulted in an amino acid substitution of glycine 12 to serine (Figure S1A). Two WT iPSC lines derived from foreskin fibroblasts (CRL-2097, ATCC, Manassas, VA) and human dermal fibroblasts were used as controls (Kim et al., 2015; Park et al., 2015). The CS iPSCs and WT iPSCs were cultured in embryonic stem cell (ESC) medium on mitomycin C-treated (A.G. Scientific, San Diego, CA) mouse embryo fibroblasts (MEFs) at a density of 1×10^4 cells/cm^2. The ESC medium consisted of DMEM/F12 (Invitrogen, Carlsbad, CA) with 20% Knockout SR (Invitrogen), 1% nonessential amino acids (Invitrogen), 1.2 mg/mL sodium carbohydrate, 0.1 mM β-mercaptoethanol (Sigma, St. Louis, MO), and 10 ng/mL basic fibroblast growth factor 2 (R&D Systems, Minneapolis, MN) at 37°C and 5% CO_2. The established CS iPSC lines were then characterized by their expression of human ESC markers (Figure S1B) and the ability to differentiate into cells of the three germ layers (Figure S1C).

Differentiation of human iPSCs into MSCs

Human iPSCs were differentiated into MSCs as previously described (Choi et al., 2017b; Mahmood et al., 2010). Briefly, human iPSC colonies were dissected into small clumps (approximately 0.5 mm × 0.5 mm in size). These clumps were transferred to uncoated Petri dishes (SPL Lifesciences, Pocheon, Korea) and incubated in EB medium for 2 days. The EB medium consisted of DMEM/F12 (Invitrogen, Carlsbad, CA) with 10% Knockout SR (Invitrogen), 1% nonessential amino acids (Invitrogen), 1.2 mg/mL sodium carbohydrate, and 0.1 mM β-mercaptoethanol (Sigma, St. Louis, MO). In this medium, the clumps spontaneously aggregated to form embryoid bodies (EBs). These EBs were cultured in the same medium

supplemented with 10 μM SB431542 (Cayman Chemical, Ann Arbor, MI) for 8 d with media changes every other day. After 10 d of incubation, the EBs were attached to fibronectin-coated dishes (BD Biosciences, Franklin Lakes, NJ) and then further cultured in DMEM/F12 supplemented with 1 μM SB431542, 1% insulin plus transferrin liquid supplement (Sigma), 2% B27 supplement (Invitrogen), and 1% CD lipid (Invitrogen) for 8–10 additional days with medium changes every other day. For MSC maturation, the cells were then cultured in α-MEM (Invitrogen) containing 10% FBS for 14 days with medium changes once every 3 days.

Differentiation of MSCs into osteoblasts

STEMPRO differentiation medium (Invitrogen) was used as a basal medium for differentiation into osteoblasts. For osteogenesis, MSCs were seeded at a density of 1×10^5 cells/cm^2. At 80% confluence, the MSCs were cultured in osteogenesis medium (the basal medium with an additional osteogenesis supplement) for 21 days with medium changes once every 3 days. The differentiation of these cells was confirmed by ALP activity, as well as AR-S and VK staining. ALP activity was visualized at 7 days of osteogenic differentiation using a Leukocyte Alkaline Phosphatase Kit (Sigma) according to the manufacturer's protocol. ALP activity was quantified with an Alkaline Phosphatase Yellow (pNPP) Liquid Substrate System (Sigma) according to the manufacturer's protocol. For AR-S staining, cells at 14 days were fixed with 10% formalin for 10 min and stained in AR-S solution (American Master Tech, Lodi, CA) at room temperature (RT) for 1 h. AR-S was extracted using cetylpyridinium chloride (CPC) in distilled water (DW) (35 mg/mL). The samples were incubated with the CPC reagent for 2 h at 4°C. The concentration of AR-S was measured via absorbance at 405 nm using a microplate reader (Thermo Fisher Scientific). For VK staining, cells at 21 days were fixed with 10% formalin for 10 min and incubated in 5% silver nitrate (American Master Tech, Lodi, CA) at RT under UV light for 1 h.

Real-time quantitative PCR

Total RNA was obtained using the easy-BLUE kit (Intron Biotechnology, Seongnam, Korea). One microgram of total RNA was reverse transcribed using the First Strand cDNA Synthesis Kit (Bioassay, Daejeon, Korea) according to the manufacturer's protocol. Real-time qPCR was performed using a 2× PCR mix comprising 40 mM Tris (pH 8.4), 0.1 M KCl, 6 mM $MgCl_2$, 2 mM dNTP, 0.4% SYBR Green (Thermo Fisher Scientific), 0.2% fluorescein (Bio-Rad, Hercules, CA), 10% DMSO, and DW. The qPCR was carried out on a CFX-Connect Real-Time System (Bio-Rad) through 30–40 cycles of 95°C denaturation, 60°C annealing, and 72°C elongation steps. The transcription level of *GAPDH* was used to normalize the expression of the target genes. The difference between the GAPDH Ct and the target Ct was used to calculate the △ threshold cycle (△Ct) value. mRNA expression fold changes between the samples and the controls were determined using the formula $2^{-(S\triangle Ct\text{-}C\triangle Ct)}$. The primers used in this study are listed in Table S2.

Immunostaining

Cells were fixed in 10% formalin solution (Sigma) at 4°C for 30 min. After being washed with PBST (PBS containing 0.1% Tween 20) three times, the cells were permeabilized in PBS supplemented with 0.1% Triton X-100 (Sigma) for 20 min with gentle agitation. The cells were then blocked with 2% BSA for 1 h and incubated at 4°C overnight after the addition of each primary antibody. After being washed with PBST three times, the cells were incubated with secondary antibodies (Alexa Fluor 488 or 594; Abcam, Cambridge, MA) at RT for 1 h. The samples were counterstained with DAPI (Sigma) and analyzed on a fluorescence microscope (Olympus, Tokyo, Japan). The primary antibodies used in this study are listed in Table S3.

Western blotting

Cells were lysed in RIPA buffer (GenDEPOT, Katy, TX) containing protease and a phosphatase inhibitor cocktail (GenDEPOT) by gentle agitation at 4°C for 2 h. Lysed cells were centrifuged at 16,000 x *g* for 15 min, and then the supernatant was collected. The protein concentration of the supernatant was measured using the Bradford protein assay (Bio-Rad). The lysate was denatured in SDS-PAGE buffer (250 mM Tris-HCl [pH 6.8] with 5% 2-mercaptoethanol, 10% SDS, 0.5% bromophenol blue, and 50% glycerol) at 95°C for 5 min. The samples (at 1 μg/μL) were loaded on a 12% SDS-PAGE gel and then transferred to a nitrocellulose membrane (Whatman, Maidstone, England). After the samples were blocked with 5% BSA or 5% skim milk in Tris-buffered saline containing 0.1% Tween 20 (TBST: 10 mM Tris-HCl [pH 7.5], 150 nM NaCl, and 0.1% Tween 20) for 1 h, they were incubated at 4°C overnight after the addition of primary antibody. The primary antibodies used in this study are listed in Table S4. The membranes were then washed with 5% TBST and incubated with a horseradish peroxidase-conjugated secondary antibody (Cell Signaling Technology, Beverly, MA) at RT for 1 h. The ECL reagent (Merck Millipore, Billerica, MA) was used for developing the membranes. The LAS-4000 Mini biomolecular imager (Fuji Film, Tokyo, Japan) was used to detect protein bands. The intensity of each band was quantified with ImageJ software (NIMH, Bethesda, MD). HRAS activity was measured using the HRAS Activation Assay Kit (Cell Biolabs, San Diego, CA) according to the manufacturer's instructions. The lysate was incubated with HRAS-GTP pull-down beads for 1 h with gentle agitation. After being washed with lysis buffer, the beads were denatured in SDS-PAGE buffer at 95°C for 5 min. Western blotting for HRAS-GTP was performed as described above.

FACS analysis

MSCs were harvested using a trypsin solution containing 0.25% EDTA (Invitrogen). After a neutralization step in FACS buffer (PBS containing 1% FBS), the cells were filtered into a cell strainer with 40 μm pores (Corning, Corning, NY). The harvested cells were centrifuged at 300 × *g* for 5 min at 4°C and washed in FACS buffer. The samples were then incubated at 4°C for 20 min in the dark with FACS antibodies against CD34, CD45, HLA-DR, CD73, CD90, or CD105. The antibodies used in the FACS analysis are listed in Table S5. After being washed with FACS buffer, the antibody-labeled cells were examined using a FACS LSRFortessa flow cytometer (BD Biosciences). MSC marker expression rates were analyzed with FlowJo software (Tree Star, Ashland, OR, USA).

Transfection

MSCs were transfected with TIMP1- or TIMP2-specific siRNAs (Santa Cruz, Dallas, TX) using the RNAimax reagent (Thermo

Fisher Scientific) according to the manufacturer's protocol. Briefly, 5×10^4 cells were suspended in 50 μL Opti-MEM (Thermo Fisher Scientific) containing 10 nM siRNA and 0.6 μL RNAimax reagent. Scrambled siRNAs (Dharmacon) were used as a negative control. MSCs (5×10^4 cells) were transfected with pCMV5b-SMAD3CA vectors (250 ng) in MSC medium (450 μL) containing 50 μL Opti-MEM and 1 μL Lipostem reagent (Thermo Fisher Scientific) at 37°C for 24 h. Then, the transfected cells were cultured in osteogenesis medium at 37°C with medium changes every 3 days. Day 7 osteoblasts were examined for ALP activity, and day 14 osteoblasts were stained with AR-S solution to measure mineralization.

Correction of $HRAS^{G12S}$ mutation in CS iPSCs by CRISPR-Cas9 system

CS iPSCs (1×10^6 cells) were transfected in Opti-MEM with 2.5 μg pCas9-GFP plasmids, 2.5 μg sgRNA plasmids, and 5 μg ssODNs using a NEPA21 electroporator (125 V, 5 s) (Nepagene, Shioyaki, Ichikawa, Japan). After electroporation, the cells were transferred to Matrigel-coated cell culture plates and cultured in mTESR medium (STEMCELL Technologies, Vancouver, BC, Canada) supplemented with 10 μM ROCK inhibitor (Y27632) at 37°C for 24 h. GFP-positive cells were sorted using a FACSAria II flow cytometer (BD Biosciences) and immediately cultured in ESC medium containing Y27632 (10 μM) and 5 μg/mL gentamycin on mitomycin C-treated MEF feeders until colony formation. Approximately 500 GFP-positive cells were plated per well in six-well plates. The colonies were harvested in lysis solution (50 mM Tris-HCl [pH 8.5], 1 mM EDTA, 0.005% SDS, 200 μg/mL proteinase K) at 50°C for 2 h. They were then heated at 95°C for 10 min to inactivate proteinase K. The genomic region around the CRISPR-Cas9 target site for the *HRAS* correction was amplified via PCR using a Taq 1.1 premix (Bioassay) with 2% Tween 20. The primers used for *HRAS* sequencing were forward, 5′-GACCTGTTCTGGAGGACG-3′, and reverse, 5′-CCTATCCTGGCTGTGTCC-3′. Of 50 individual clones, 10 had indel mutations and 1 showed correction of $HRAS^{G12S}$ with normal expression of pluripotency-associated markers (Figure S5A). The potential off-target sites of the sgRNA were examined by using the RGEN tool. The PCR primers for detecting mutations in potential off-target sites are listed in Table S6.

Statistics

The n value means independent experiments as biological replicates. We performed all experiments with independently differentiated cells from WT and CS iPSCs. All data collected from experiments were used for analysis in this study. Each experiment was repeated at least three times. Data obtained from experiments in which SMAD3CA was overexpressed in WT iPSCs or those using the corrected CS iPSCs are presented as means ± SD. The data obtained from all other experiments are presented as means ± SEM. In each case the mean of the dataset obtained from the two WT cell lines was compared with the mean of the dataset obtained from the three CS lines. Statistical significance was evaluated using a two-tailed Student t test performed with GraphPad Prism 7 (GraphPad Software, La Jolla, CA). The p values are indicated as follows: $*p \leq 0.05$, $**p \leq 0.01$, $***p \leq 0.001$.

SUPPLEMENTAL INFORMATION

Supplemental information can be found online at https://doi.org/10.1016/j.stemcr.2021.06.007.

AUTHOR CONTRIBUTIONS

J.B.C.: conception, design, assembly data, data analysis, interpretation, and manuscript writing. J.S.L. and M.Y.K.: support for establishment of CS1 iPSCs. B.S.K., Y.H.J., and H.S.D.: design and interpretation. H.W.Y. and B.H.L.: provision of CS dermal fibroblasts and the clinical information of CS patients. Y.M.H.: management of the project and manuscript writing. All authors agree to the authorship.

CONFLICTS OF INTEREST

The authors declare no competing interests.

ACKNOWLEDGMENTS

We are grateful to the Flow Cytometry core facility in KAIST. This research was supported by a grant (2018M3A9H1078330) from the National Research Foundation (NRF) of the Republic of Korea.

Received: January 28, 2021
Revised: June 8, 2021
Accepted: June 9, 2021
Published: July 8, 2021

REFERENCES

Alliston, T., Choy, L., Ducy, P., Karsenty, G., and Derynck, R. (2001). TGF-beta-induced repression of CBFA1 by Smad3 decreases cbfa1 and osteocalcin expression and inhibits osteoblast differentiation. EMBO J. *20*, 2254–2272.

Almalki, S.G., and Agrawal, D.K. (2016). Effects of matrix metalloproteinases on the fate of mesenchymal stem cells. Stem Cell Res. Ther. *7*, 12.

Aoki, Y., Niihori, T., Kawame, H., Kurosawa, K., Ohashi, H., Tanaka, Y., Filocamo, M., Kato, K., Suzuki, Y., Kure, S., et al. (2005). Germline mutations in HRAS proto-oncogene cause Costello syndrome. Nat. Genet. *37*, 1038–1040.

Boskey, A.L. (2013). Bone composition: relationship to bone fragility and antiosteoporotic drug effects. Bonekey Rep. *2*, 447.

Bruder, S.P., Fink, D.J., and Caplan, A.I. (1994). Mesenchymal stem cells in bone development, bone repair, and skeletal regenaration therapy. J. Cell. Biochem. *56*, 283–294.

Chen, C.G., Thuillier, D., Chin, E.N., and Alliston, T. (2012). Chondrocyte-intrinsic Smad3 represses Runx2-inducible matrix metalloproteinase 13 expression to maintain articular cartilage and prevent osteoarthritis. Arthritis Rheum. *64*, 3278–3289.

Choi, H., Kim, T.-H., Yang, S., Lee, J.-C., You, H.-K., and Cho, E.-S. (2017a). A reciprocal interaction between β-catenin and osterix in cementogenesis. Sci. Rep. *7*, 8160.

Choi, J.Y., Han, K.M., Kim, D., Lee, B.H., Yoo, H.W., Choi, J.H., and Han, Y.M. (2017b). Impaired osteogenesis of disease-specific

induced pluripotent stem cells derived from a CFC syndrome patient. Int. J. Mol. Sci. *18*, 2591.

Costello, J.M. (1977). New syndrome - mental-subnormality and nasal papillomata. Aust. Paediatric J. *13*, 114–118.

Day, T.F., Guo, X., Garrett-Beal, L., and Yang, Y. (2005). Wnt/beta-catenin signaling in mesenchymal progenitors controls osteoblast and chondrocyte differentiation during vertebrate skeletogenesis. Dev. Cell *8*, 739–750.

Ducy, P., Zhang, R., Geoffroy, V., Ridall, A.L., and Karsenty, G. (1997). Osf2/Cbfa1: a transcriptional activator of osteoblast differentiation. Cell *89*, 747–754.

Egea, V., Zahler, S., Rieth, N., Neth, P., Popp, T., Kehe, K., Jochum, M., and Ries, C. (2012). Tissue inhibitor of metalloproteinase-1 (TIMP-1) regulates mesenchymal stem cells through let-7f microRNA and Wnt/β-catenin signaling. Proc. Natl. Acad. Sci. U S A *109*, E309–E316.

Felber, K., Elks, P.M., Lecca, M., and Roehl, H.H. (2015). Expression of osterix is regulated by FGF and Wnt/β-catenin signalling during osteoblast differentiation. PLoS One *10*, e0144982.

Goodwin, A.F., Tidyman, W.E., Jheon, A.H., Sharir, A., Zheng, X., Charles, C., Fagin, J.A., McMahon, M., Diekwisch, T.G., Ganss, B., et al. (2014). Abnormal Ras signaling in Costello syndrome (CS) negatively regulates enamel formation. Hum. Mol. Genet. *23*, 682–692.

Hennekam, R.C.M. (2003). Costello syndrome: an overview. Am. J. Med. Genet. C Semin. Med. Genet. *117C*, 42–48.

Holmbeck, K., Bianco, P., Caterina, J., Yamada, S., Kromer, M., Kuznetsov, S.A., Mankani, M., Robey, P.G., Poole, A.R., Pidoux, I., et al. (1999). MT1-MMP-deficient mice develop dwarfism, osteopenia, arthritis, and connective tissue disease due to inadequate collagen turnover. Cell *99*, 81–92.

Hua, X., Miller, Z.A., Wu, G., Shi, Y., and Lodish, H.F. (1999). Specificity in transforming growth factor β-induced transcription of the plasminogen activator inhibitor-1 gene: interactions of promoter DNA, transcription factor μE3, and Smad proteins. Proc. Natl. Acad. Sci. *96*, 13130–13135.

Kasper, G., Dankert, N., Tuischer, J., Hoeft, M., Gaber, T., Glaeser, J.D., Zander, D., Tschirschmann, M., Thompson, M., Matziolis, G., et al. (2007). Mesenchymal stem cells regulate angiogenesis according to their mechanical environment. Stem Cells *25*, 903–910.

Kim, D., Choi, J., Han, K.M., Lee, B.H., Choi, J.H., Yoo, H.W., and Han, Y.M. (2015). Impaired osteogenesis in Menkes disease-derived induced pluripotent stem cells. Stem Cell. Res. Ther. *6*, 160.

Krencik, R., Hokanson, K.C., Narayan, A.R., Dvornik, J., Rooney, G.E., Rauen, K.A., Weiss, L.A., Rowitch, D.H., and Ullian, E.M. (2015). Dysregulation of astrocyte extracellular signaling in Costello syndrome. Sci. Transl. Med. *7*, 286ra266.

Krishnan, V., Bryant, H.U., and Macdougald, O.A. (2006). Regulation of bone mass by Wnt signaling. J. Clin. Invest. *116*, 1202–1209.

Leivonen, S.K., Lazaridis, K., Decock, J., Chantry, A., Edwards, D.R., and Kähäri, V.M. (2013). TGF-β-elicited induction of tissue inhibitor of metalloproteinases (TIMP)-3 expression in fibroblasts involves complex interplay between Smad3, p38α, and ERK1/2. PLoS One *8*, e57474.

Leoni, C., Stevenson, D.A., Martini, L., De Sanctis, R., Mascolo, G., Pantaleoni, F., De Santis, S., La Torraca, I., Persichilli, S., Caradonna, P., et al. (2014). Decreased bone mineral density in Costello syndrome. Mol. Genet. Metab. *111*, 41–45.

Liu, B., Wu, S., Han, L., and Zhang, C. (2015). β-catenin signaling induces the osteoblastogenic differentiation of human pre-osteoblastic and bone marrow stromal cells mainly through the upregulation of osterix expression. Int. J. Mol. Med. *36*, 1572–1582.

Liu, L., Liu, X., Ren, X., Tian, Y., Chen, Z., Xu, X., Du, Y., Jiang, C., Fang, Y., Liu, Z., et al. (2016). Smad2 and Smad3 have differential sensitivity in relaying TGFβ signaling and inversely regulate early lineage specification. Sci. Rep. *6*, 21602.

Lu, P., Takai, K., Weaver, V.M., and Werb, Z. (2011). Extracellular matrix degradation and remodeling in development and disease. Cold Spring Harb. Perspect. Biol. *3*, a005058.

Mahmood, A., Harkness, L., Schroder, H.D., Abdallah, B.M., and Kassem, M. (2010). Enhanced differentiation of human embryonic stem cells to mesenchymal progenitors by inhibition of TGF-beta/activin/nodal signaling using SB-431542. J. Bone Miner. Res. *25*, 1216–1233.

Mosig, R.A., Dowling, O., DiFeo, A., Ramirez, M.C.M., Parker, I.C., Abe, E., Diouri, J., Aqeel, A.A., Wylie, J.D., Oblander, S.A., et al. (2007). Loss of MMP-2 disrupts skeletal and craniofacial development and results in decreased bone mineralization, joint erosion and defects in osteoblast and osteoclast growth. Hum. Mol. Genet. *16*, 1113–1123.

Mott, J.D., and Werb, Z. (2004). Regulation of matrix biology by matrix metalloproteinases. Curr. Opin. Cell Biol. *16*, 558–564.

Nakashima, K., Zhou, X., Kunkel, G., Zhang, Z., Deng, J.M., Behringer, R.R., and de Crombrugghe, B. (2002). The novel zinc finger-containing transcription factor osterix is required for osteoblast differentiation and bone formation. Cell *108*, 17–29.

Nistala, H., Lee-Arteaga, S., Smaldone, S., Siciliano, G., Carta, L., Ono, R.N., Sengle, G., Arteaga-Solis, E., Levasseur, R., Ducy, P., et al. (2010). Fibrillin-1 and -2 differentially modulate endogenous TGF-β and BMP bioavailability during bone formation. J. Cell Biol. *190*, 1107–1121.

Ozeki, N., Mogi, M., Hase, N., Hiyama, T., Yamaguchi, H., Kawai, R., and Nakata, K. (2016). Polyphosphate-induced matrix metalloproteinase-13 is required for osteoblast-like cell differentiation in human adipose tissue derived mesenchymal stem cells. Biosci. Trends *10*, 365–371.

Page-McCaw, A., Ewald, A.J., and Werb, Z. (2007). Matrix metalloproteinases and the regulation of tissue remodelling. Nat. Rev. Mol. Cell Biol. *8*, 221–233.

Park, H.J., Choi, Y.J., Kim, J.W., Chun, H.S., Im, I., Yoon, S., Han, Y.M., Song, C.W., and Kim, H. (2015). Differences in the epigenetic regulation of cytochrome P450 genes between human embryonic stem cell-derived hepatocytes and primary hepatocytes. PLoS One *10*, e0132992.

Rydziel, S., Varghese, S., and Canalis, E. (1997). Transforming growth factor β1 inhibits collagenase 3 expression by transcriptional and post-transcriptional mechanisms in osteoblast cultures. J. Cell. Physiol. *170*, 145–152.

Saw, S., Aiken, A., Fang, H., McKee, T.D., Bregant, S., Sanchez, O., Chen, Y., Weiss, A., Dickson, B.C., Czarny, B., et al. (2019). Metalloprotease inhibitor TIMP proteins control FGF-2 bioavailability and regulate skeletal growth. J. Cell Biol. *218*, 3134–3152.

Schindeler, A., and Little, D.G. (2006). Ras-MAPK signaling in osteogenic differentiation: friend or foe? J. Bone Miner. Res. *21*, 1331–1338.

Takahashi, K., Tanabe, K., Ohnuki, M., Narita, M., Ichisaka, T., Tomoda, K., and Yamanaka, S. (2007). Induction of pluripotent stem cells from adult human fibroblasts by defined factors. Cell *131*, 861–872.

Tidyman, W.E., and Rauen, K.A. (2009). The RASopathies: developmental syndromes of Ras/MAPK pathway dysregulation. Curr. Opin. Genet. Dev. *19*, 230–236.

Verrecchia, F., and Mauviel, A. (2002). Transforming growth factor-beta signaling through the Smad pathway: role in extracellular matrix gene expression and regulation. J. Invest. Dermatol. *118*, 211–215.

Vu, T.H., and Werb, Z. (2000). Matrix metalloproteinases: effectors of development and normal physiology. Genes Dev. *14*, 2123–2133.

Wipff, P.J., and Hinz, B. (2008). Integrins and the activation of latent transforming growth factor beta1 - an intimate relationship. Eur. J. Cell Biol. *87*, 601–615.

Wu, M., Chen, G., and Li, Y.-P. (2016). TGF-β and BMP signaling in osteoblast, skeletal development, and bone formation, homeostasis and disease. Bone Res. *4*, 16009.

Xia, Y., and Wu, S. (2015). Tissue inhibitor of metalloproteinase 2 inhibits activation of the β-catenin signaling in melanoma cells. Cell Cycle *14*, 1666–1674.

Yan, Y., Tang, D., Chen, M., Huang, J., Xie, R., Jonason, J.H., Tan, X., Hou, W., Reynolds, D., Hsu, W., et al. (2009). Axin2 controls bone remodeling through the beta-catenin-BMP signaling pathway in adult mice. J. Cell Sci. *122*, 3566–3578.

Yao, F., He, Z., Lu, M., Li, P., and Wang, J. (2017). Smad2 and Smad3 Play Differential Roles in the Regulation of Matrix Deposition-Related Enzymes in Renal Mesangial Cells.

Zhang, C., Tang, W., and Li, Y. (2012). Matrix metalloproteinase 13 (MMP13) is a direct target of osteoblast-specific transcription factor osterix (Osx) in osteoblasts. PLoS one *7*, e50525.